

Nanoscale

Accepted Manuscript



This is an *Accepted Manuscript*, which has been through the Royal Society of Chemistry peer review process and has been accepted for publication.

Accepted Manuscripts are published online shortly after acceptance, before technical editing, formatting and proof reading. Using this free service, authors can make their results available to the community, in citable form, before we publish the edited article. We will replace this *Accepted Manuscript* with the edited and formatted *Advance Article* as soon as it is available.

You can find more information about *Accepted Manuscripts* in the [Information for Authors](#).

Please note that technical editing may introduce minor changes to the text and/or graphics, which may alter content. The journal's standard [Terms & Conditions](#) and the [Ethical guidelines](#) still apply. In no event shall the Royal Society of Chemistry be held responsible for any errors or omissions in this *Accepted Manuscript* or any consequences arising from the use of any information it contains.



Nanoscale

ARTICLE

Strain-tuned optoelectronic property of hollow gallium sulphide microsphere

Received 00th January 2015,
Accepted 00th January 2015

DOI: 10.1039/x0xx00000x

Yin Zhang,[†] Chen Chen,[†] C. Y. Liang, Z. W. Liu, Y. S. Li, and Renchao Che*

www.rsc.org/Nanoscale

Sulfide semiconductors have been attracting extensive attentions. The main challenge requests a solution to prepare the materials with designable morphology, controllable band structure and optoelectronic properties. Herein, we report a facile chemical transportation reaction for Ga₂S₃ microspheres with novel hollow morphologies and partially filled volume. Even without any extrinsic element dopant, photoluminescence (PL) emission wavelength could be facilely tuned from 635 to 665 nm, determined by its intrinsic inhomogeneous strain distribution. Geometric phase analysis (GPA) based on high-resolution transmission electron microscopy (HRTEM) imaging reveals that the strain distribution and the associated PL properties can be accurately controlled by changing the growth temperature gradient, which depends on the distance between the boats used for raw material evaporation and microsphere deposition. The stacking-fault density, lattice distortion degree and strain distribution at the shell interfacial region of Ga₂S₃ microsphere could be readily adjusted. Ab initio first-principle calculations confirm that the lowest conductive band (LCB) is dominated by S-3s and Ga-4p states, which shifts to low-energy band by the introduction of tensile strain, according well with the observed PL evolution. Therefore, based on our strain driving strategy, a novel guideline toward the reasonable design of sulfide semiconductors with tunable photoluminescence property is proposed.

Introduction

Sulfides, such as Ga₂S₃, ZnS and CdS, have been highly desirable in various semiconductor industry fields of photocatalysis, light-emission, fluorescence biology and energy-harvesting devices, mainly due to the designable band structure.¹⁻³ However, there are still great problems when most sulfide semiconductor materials are used as actual devices, including quality uniformity during massive yield, structure collapse caused by residual strain, unstable phase structure exposed under oxygenic/acid environment and

vanishing of quantum confinement effect.⁴⁻⁷ To solve the above issues, metallic sulfide semiconductors with versatile morphologies and desirable band structure, such as nanodot, nanorod, nanosheet, film and microsphere,^{4, 8-15} have been developed. However, the inevitable stacking faults and twin boundaries of sulfide semiconductors could sensitively alter the band structure and optical property.^{4, 12, 13} These crystalline defect should be controlled within an optimized density level and moreover be utilized as “band engineering”. Otherwise, optoelectronic properties will be irreversibly degraded.

Ga₂S₃ is expected to be a promising kind of blue-light-emitting semiconductor.¹⁶ However, only a few works on the association between its luminescent property and microstructure have been reported.^{16, 17} Layered Ga₂S₃ structure with Cc and F43m symmetry has been synthesized and expected to embrace infrared nonlinear property.^{4, 11-13} Regarding the growth and band design, although a considerable amount of literatures about sulfides are available, many of them only emphasize morphology adjustment and elemental dopant rather than from the viewpoint of atomic level design. As far as we know, there are

Laboratory of Advanced Materials, Department of Materials Science and Collaborative Innovation Center of Chemistry for Energy Materials, Fudan University, Shanghai 200438, People's Republic of China, Tel.: (+86)-21-51630213, E-mail: rcche@fudan.edu.cn

[†] These authors contributed equally to this work.

Electronic Supplementary Information (ESI) available: [crystal structure pattern; calculated DOS diagram]. See DOI: 10.1039/x0xx00000x

ARTICLE

Nanoscale

few reports discussing about the connection between the microstructure and the photoelectric properties of gallium sulfide semiconductor, which is urgently requested to enrich the current fabrication strategy. Information about the local strain and defects such as stacking faults of the whole semiconductor device is of critical importance in regulating the band structure and the photoelectric properties. But the mechanism behind the influences of lattice imperfections on device performance still remains unclear. So far, a comprehensive design framework, used for shedding light on the controllable fabrication of the crystal defects, energy gaps, local energy bands, and surface electron states, is urgently needed but still unavailable.

Herein, we have developed a novel growth strategy for a series of Ga₂S₃ hollow microspheres with tunable morphology and adjustable emission wavelength, controlled by the designable strain distribution. It is striking to observe that PL emission wavelength can be sensitively modulated by the strain system within the shell region, which critically depends on the deposition temperature and the associated lattice distortion. HRTEM imaging shows that two types of defects exist in the crystal structure: stacking fault (SF) and the spot defect (SD). GPA shows that SF cause a very wide regional strain distribution in the structure. It is further confirmed to have influence on the density of states (DOS) and the band structure (BS) by *ab initio* calculation. Lower deposition temperature helps the samples with perfect morphology but also increases the strain density. All the results suggest that this novel strain-adjusting strategy may become an attractive approach for tuning optoelectronic properties of sulfide semiconductors.

Experimental Section

Synthesis

The Ga₂S₃ samples were fabricated through a chemical transportation reaction process. Pure Ga₂O₃ powder was placed in the quartz boat where the temperature was set at 1150±0.1 °C for evaporation. Silicon (111) wafer was cleaned beforehand through a standard RCA cleaning process and placed upon four Al₂O₃ boats in the downstream side as a substrate for collecting the sample. During growth the temperature of the four substrates were kept at 950, 900, 850 and 800 °C, respectively. Ga₂O₃ powder was put inside the center of the first boat and sulfur source was provided by flowing a stream of H₂S (10%)/Ar₂ (90%) carrier gas (flowing rate is 300 sccm at 15 mbar) into the horizontal furnace, according to the method described as Ref. [6]. One hour later, a layer of white powder could be obtained from each substrate. After the deposition, samples were left in the furnace over night for cooling down.

Materials Characterizations

Photoluminescence (PL) measurements were carried out on an Edinburgh FLS980 fluorescence spectrometer. The crystalline phase of the product was examined by an X-ray diffractometer (Bruker D8 Advance) using Cu K_α radiation (λ=1.542 Å). The morphologies of the products were characterized by a scanning electron microscope (SEM, HITACHI S-4800) operated at 1.0 kV. The microstructure and

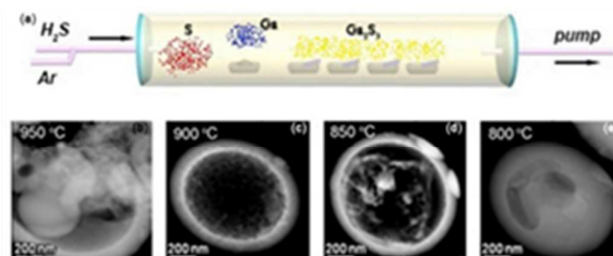


Fig. 1 (a) Schematic diagram of growth process showing the positions of the precursors and the substrate inside the furnace. (b-e) TEM images exhibits the four types of Ga₂S₃ spheres from various temperature.

crystal lattice were analyzed on a JEOL JEM-2100F transmission electron microscope (TEM) equipped with a post-column Gatan imaging filter (GIF-Tridium) at 200 kV acceleration voltage. The digital micrograph software (Gatan) was used for image recording/processing. For TEM studies, samples were scrapped out from the substrates, thoroughly dispersed in 2-propanol and then several drops were deposited on a carbon coated copper grid.

GPA Method and Calculation

GPA was performed to mapping the strain distributions across the structure of all the samples. The displacements in the Fourier-filtered local image pattern relative to an internal reference area is analyzed with respect to a shift in the atomic positions. The in-plane strain tensor components, ϵ_{xx} , ϵ_{yy} , ϵ_{xy} , can thus be obtained from the local structural displacements u by numerical/partial differentiation:

$$\epsilon_{xx} = \frac{\partial u_x}{\partial x}, \epsilon_{yy} = \frac{\partial u_y}{\partial y}, \epsilon_{xy} = \frac{1}{2} \left(\frac{\partial u_x}{\partial y} + \frac{\partial u_y}{\partial x} \right)$$

A commercial version, GPA Phase 4.0 (HREM Research), which is based on the formalism given in Ref. [18] and implemented in Digital Micrograph (Version 1.71.38, Gatan) as a plug-in, was used to calculate the in-plane components of the symmetric strain tensor, ϵ_{xx} , ϵ_{yy} , ϵ_{xy} , using high-resolution micrographs of the samples. The full potential linearized augmented-plane-wave+local orbital simulation (APW+LO) were used as implement in WIEN 2k code. The $R_{mt}K_{max}$ was set to be 7.5 to determine the basis size for spreading the plane wave. For the self-consistent calculations in all four cases, the energy, charge, and force were converged to be 10^{-5} Ry, 10^{-4} e, and 1 mRy/au, respectively. The self-consistency was

carried out on 1000 total k-points, which corresponded to a $20 \times 20 \times 9$ k-mesh in the irreducible Brillouin zone.

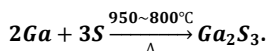
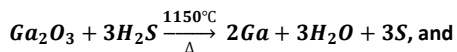
Results and Discussion

The schematic diagram of the growth process for Ga_2S_3 microspheres is illustrated in Fig. 1.



Fig. 2 Reaction mechanism showing the three stages of the Ga_2S_3 microsphere growth: deposition, reunion and ripening.

The basic chemical reactions happened in the furnace tube can be categorized into both thermal evaporation reaction and transportation deposition reaction, respectively at the first boat and silicon substrate. The associated reaction equations are:



At the first Al_2O_3 boat, gallium atoms are released by the "attacking" from H_2S gas into Ga_2O_3 during the decomposition process resulted from heating up. Immediately, atom clusters of gallium and sulfur are transported downstream by carrier gas onto silicon substrate surface for the combination of Ga_2S_3 . As the reaction continues, several types of Ga_2S_3 samples with various fluffy morphologies are formed inside the substrate surface. Interestingly, with the deposition temperature continuously decreasing from 950 to 800 °C, the morphology of the products collected at the four different positions (Fig. 1a) changes remarkably from corrupted microspheres with partly filled volume to full-filled microspheres (Fig. 1b - e). Samples of 900, 850 and 800 °C have smooth external surface and a uniform diameter of ~800 nm, whereas, sample of 950 °C are broken balls. TEM analysis exhibits different inner structures. Therefore, the temperature of silicon substrate surface where the products deposited plays an

important role in the formation of Ga_2S_3 microstructure morphology.

Ostwald ripening is widely used in the change of an inhomogeneous structure over time in solid solutions or liquid colloid.¹⁸ Here the growth process for Ga_2S_3 microsphere is similar to the Ostwald ripening model, which is based on the theory that smaller clusters/species tend to be absorbed by or re-deposited on bigger spheres (Fig. 2).

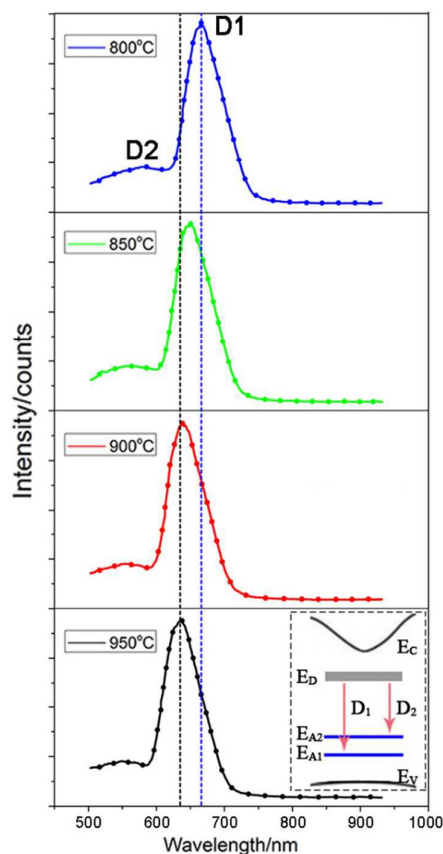


Fig. 3 PL spectrum of four samples. With the growth temperature decreasing from 950 °C to 800 °C, the center of the PL peak shifts from 635 nm to 665 nm. Inset is the possible transition mechanism for the defects emissions in Ga_2S_3 .

At higher temperature, the growing speed is so fast that the ripening process has no enough time for a perfect completion, leading to the corruption of microspheres. It should be mentioned

ARTICLE

Nanoscale

that the source concentrations (Ga, H₂S) used here are higher than usual, which creates a “supersaturated” reaction environment, which is favorable for free molecules to condense on the surface of larger Ga₂S₃ spheres. Therefore, it is concluded that different deposition temperatures, which turn out to be the dominant factor for Ostwald ripening, could sensitively modify the morphology of the products.

monoclinic Ga₂S₃ structure is likely to form two acceptor bands (E_{A1} and E_{A2}) located inside the band gap (Fig. 3 inset).¹⁷ Thus two emissions D1 and D2 are attributed to the electron transition from E_D to E_{A1} and E_{A2}. With the deposition temperature decreasing from 950 °C to 800 °C, a red-shift tendency from 635 nm to 665 nm was evidently identified. It is assumed that microstructure of various sphere morphology might be responsible for this red-shift, which could facily be achieved by changing deposition temperature.

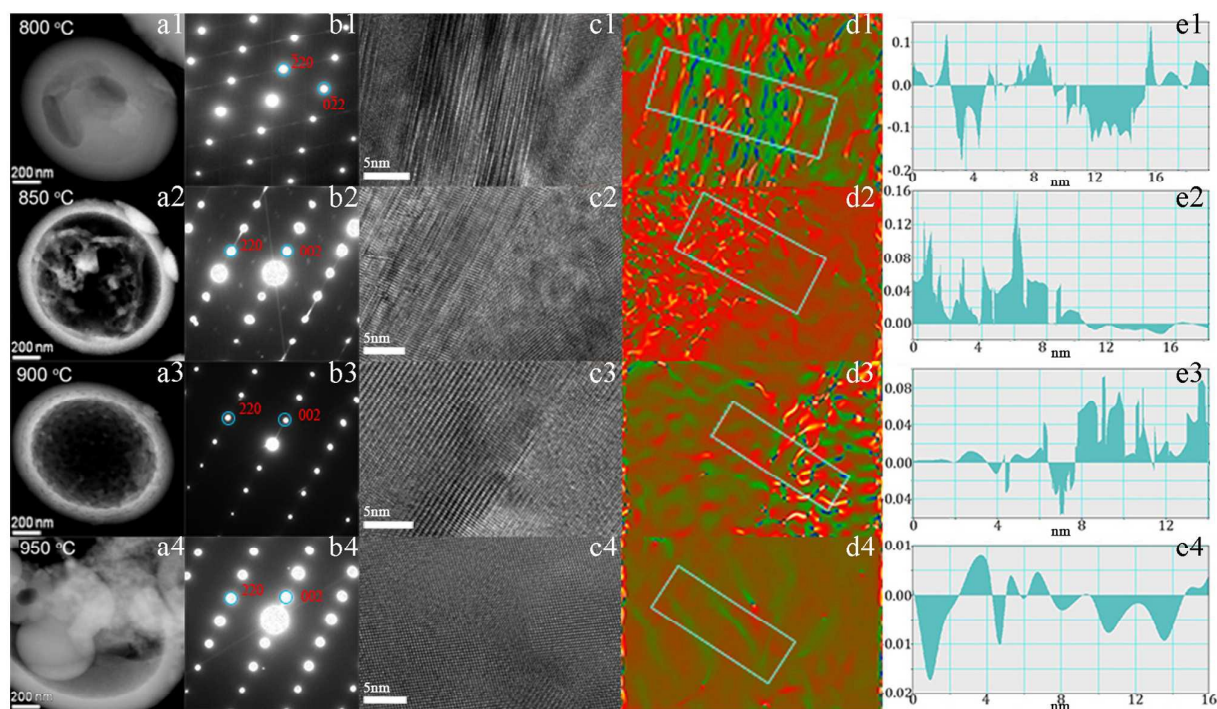


Fig. 4 (a1~a4) STEM images of the four samples. (b1~b4) ED of four samples. (c1~c4) HRTEM images in the interface area of four samples. (d1~d4) The mean dilatation of (c). Strains are shown on a scale ranging from -50% to +50% to have an optimal balanced contrast between strained and unstrained areas. Considerable strain (blue/red/yellow colors) is noticed in the form of remained stacking faults. (e1~e4) The strain distribution of the mean dilatation in the matrix was measured in the form of a profile along the length of the central matrix segment and averaged over the width of the box shown in (d).

Fig. 3 shows the photoluminescence (PL) emission dependency on the morphology of the as-prepared Ga₂S₃ microspheres. Two dominant electron transitions from donor levels to the acceptor levels are observed from all of the four samples, which centered at ~1.62 eV (D1) and ~2.12 eV (D2) for the sample of 950 °C (Fig. 3). Excitation energy of the intrinsic emission of monoclinic Ga₂S₃ crystal locates dominantly at 3.04 eV,¹⁶ indicating both D1 and D2 peaks could be ascribed to the transitions between defect bands. The sulfur vacancies form a defect donor band (E_D), whereas the ordered Ga-vacancies of gallium atoms existed in the basic

Briefly, an association between growth temperature and PL emission wavelength is readily established. Strain can always tune the band structure of semiconductor and thus modify their optical and electronic properties. Therefore, combined techniques of HRTEM imaging, electron diffraction and GPA analysis were performed for all of the four as-prepared samples, in order to clarify the dependency of strain distribution on the different morphology of Ga₂S₃ microspheres (Fig. 4). At the growth temperature of 950 °C, this sample has the highest degree of crystal perfection, without any remarkable structural defects. Even if its morphology is an incomplete sphere, it exhibits a standard monoclinic Ga₂S₃ crystal

structure (Cc space group), with a standard ABC stacking sequence along [110] orientation (Fig. S1†).

With the growth temperature decreasing, the standard ABC stacking sequence becomes more disordered, resulted from the occurrence of high density of SFs inside the original Ga₂S₃ lattice matrix. It should be mentioned that our Ga₂S₃ microspheres resulted from a combined intergrowth routine of ABC alternating stacking and embedded small domains rather than a standard epitaxial growth. Moreover, the interfacial region has a natural tendency to absorb higher density of SFs to make the whole sphere system stay at a lowest energy balance.

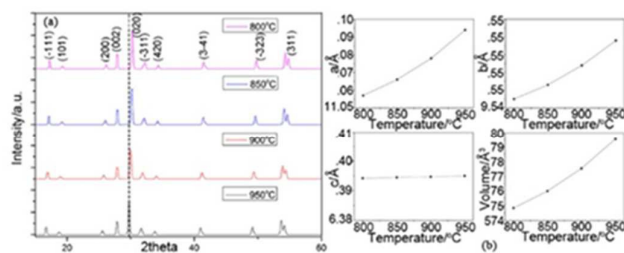


Fig. 5 (a) XRD patterns of four specimens, indexed to the monoclinic Ga₂S₃ (PDF Card no. 48-1432); (b) Dependency of lattice parameter a, b, c, and unit cell volume V on the growth temperature, respectively.

Based on the four ED patterns along zone axes of [111] and $[\bar{1}10]$, a stripe of diffraction spots with weaker contrast can be found between the main Bragg diffraction spots (002, $0\bar{2}2$), resulted from the additional incommensurable reflections contributed by the high density of SFs (Fig. 4b). SFs represents one or several pieces of Ga/S atoms was abnormally inserted or extracted from the basic Ga₂S₃ matrix periodically. Reasonably, such defect feature could play a key role in the strain distribution of our samples.

The method of GPA, developed by Martin Hÿtch, provides a powerful tool for quantitative strain measurement as revealed in HRTEM images.¹⁹⁻²¹ It should be noticed that the measurements are restricted to the in-plane components and are exterior to dislocation cores. Fig. 4d illustrates the mean dilatation of the SF area (average of strain tensor components = $(\epsilon_{xx} + \epsilon_{yy})/2$), with the brown color indicating the unstrained area and the dark color indicating the strained area. The strain distribution of the mean dilatation in the matrix was measured in the form of a profile along the length of the central matrix segments and averaged over the width of the box (Fig. 4e). For the samples of 800, 850, 900 and 950 °C, it reveals an average value of 5.8%, 4.1%, 3.3%, and 0.6%, respectively. The SFs converge predominantly around the interfacial area, while the SD scattered in other region away from interface.

Taking the sample of 950 °C as an example, there is only a few inhomogeneous strained area showing the existence of SDs (Fig. 4d4). From the line-profile of the strain maps (Fig. 4e), it can be concluded that the averaged tensile strain in interfacial area diminishes as the deposition temperature increases.

In general, two factors determine the strain distribution in the Ga₂S₃ matrix. One is the stacking faults, which might come from the merging process of small piles of Ga₂S₃ during stacking growth. The other is the SD such as ionic vacancy or displacement, which is restricted within limited area. Both SF and SD can store strain and can further modify electron band structure. Higher substrate temperature assists the merging of Ga₂S₃ piles and the dissipating of the boundary, similar to resembling an annealing process for defects, and reduces the SF concentration. Meanwhile, the SD density increases along with higher growth temperature. It should be mentioned that Ga₂S₃ sphere might lead to distortion due to the curvature surface itself, which might have influence on the strain distribution. The diameter of our Ga₂S₃ sphere is large enough (several hundreds of nanometers) that the curvature degree of them is neglectable. Even though, the strain induced by the curvature was already considered in the process of building lattice model of strained Ga₂S₃ sphere.

Fig. 5a shows the X-ray diffraction (XRD) patterns of all the four Ga₂S₃ specimens. All the detected diffraction peaks in these patterns could be well indexed on the basis of the known monoclinic Ga₂S₃ structure with a Cc space group (JCPDS card no. 48-1432). No characteristic peaks of GaS impurities can be detected. By an overdose of H₂S used in the upstream flow, Ga₂S₃ phase with high purity was successfully obtained without GaS. Through the analysis of XRD data (by JADE and Cerius² software), all of the XRD peaks shifted towards the low angle direction with the deposition temperature decreasing. The lattice parameter of sample (950 °C) comply quite well with literatures. But with the deposition temperature decrease, the lattice parameters, a, b, and lattice volume increase as well (Fig. 5b). It should be mentioned that lattice change would definitely alter the band structure of Ga₂S₃.

Analyzing the influence of lattice distortion on band structure is critical to understanding how to improve its performance in actual device applications. By the different lattice parameters extracted out from XRD patterns, four models corresponding to different growth temperatures are built up for the purpose of simulating DOS and BS.

According to the XRD data, the lattice parameters of the sample grown at 950 °C agree well with the reported values, indicating an unstrained structure. The calculated band structures of monoclinic Ga₂S₃ are plotted along the high symmetry lines of a lattice (Fig. 6a). Fig. 6a shows a direct band gap of 1.99 eV, which are smaller than the experimental observations (2.80 eV) owing to the inaccurate

description of the eigenvalues of the electronic states in GGA. The total densities of states (TDOS) of unstrained Ga_2S_3 are shown in Fig. 7d. For monoclinic Ga_2S_3 , the highest valence band (HVB) derives mainly from S-3p and Ga-4p states, whereas the lowest conduction band (LCB) is composed of Ga-4s and S-3p states (Fig. S2[†]). The valence bands (VBs) spanning over -7.3 and -4.7 eV originate predominately from Ga-4s and S-3p states. The conduction bands (CBs) ranging from 4.2 to 8.0 eV mainly consist of Ga-4p and S-3p states with a small portion of Ga-3d states. The CBs from 8.0 to 20.0 eV are mostly contributed from Ga-4p, Ga-3d and S-3p states. Briefly, the energy gaps are mainly determined by the

It is well known that band structure could be altered by the tensile/compression strain existed inside the lattice matrix.^{22,23} By taking the strain into account, the calculated TDOS of all the four samples are plotted in Fig. 7. The Ga-S bond length increases under the tensile strain, and weakens the electron coupling between the S-3p and G-4p orbits (Fig. 4e). While no obvious change can be found from the valence bands of samples gathered at various deposition temperatures, the conduction band shifts towards the low energy direction, which mainly owing to the change of S-3p and G-4p orbits. The sample at 950 °C has a band gap of 1.86 eV, while other samples at 900 °C, 850 °C and 800 °C have band gaps of 1.79, 1.74, 1.68 eV, respectively (Fig. 6b-d). The variation of band gap is

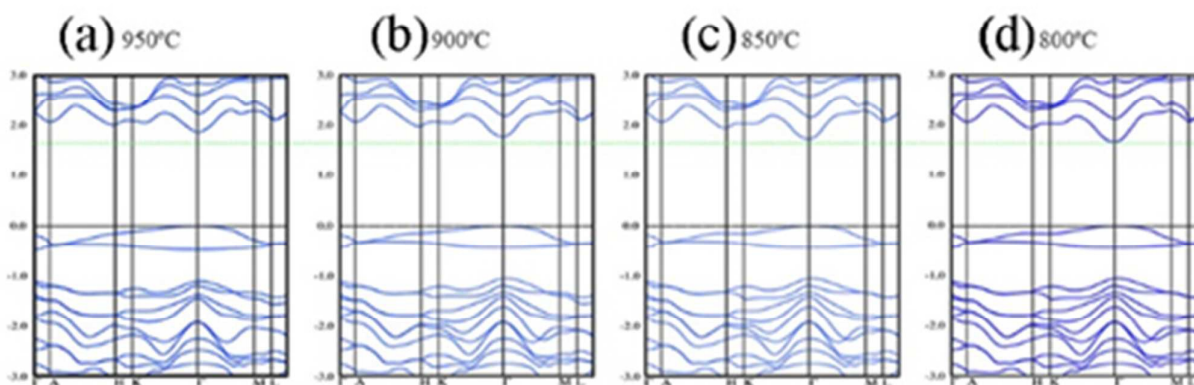


Fig. 6 Band structures of four samples grown at (a) 950 °C, (b) 900 °C, (c) 850 °C, (d) 800 °C. The direct band gap is decreasing while the deposition temperature decrease.

S-3p, Ga-4s and Ga-4p states.

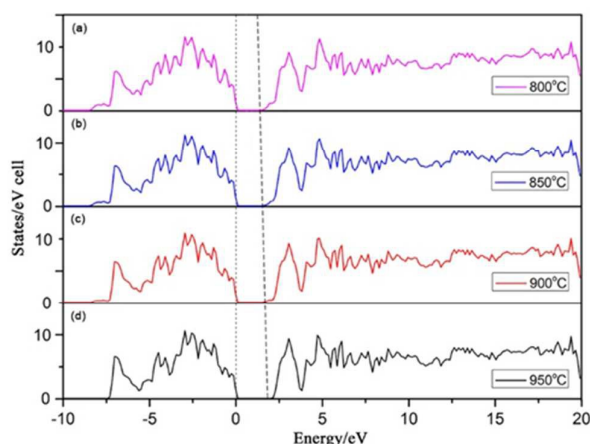


Fig. 7 TDOS of four Ga_2S_3 spheres grown at (a) 800 °C, (b) 850 °C, (c) 900 °C, (d) 950 °C, respectively.

about 9.7% from the unstrained structure (950 °C) to the most strained one (800 °C), which has a close affinity to the PL shift (3.1%). This difference is resulted from that actual SFs is difficult to be included in our simulation model due to the limited computation power. Only the simplified tensile strain caused by SF has been considered.

Conclusions

Based on the novel strategy of tuning the intrinsic strain, we develop a series of strained Ga_2S_3 hollow micro-spheres with controllable morphology and adjustable emission wavelength. The optimized approach is to change the distance between the raw material evaporation and growth substrate, equal to varying the deposition temperature, which can be facily used to control the strain level within the sphere shell region. With the strain level increasing, red-shifting can be observed from the PL emission spectrum, governed by the higher density of SFs and strain. Furthermore, both stacking faults and spot defect have been directly imaged inside all of the Ga_2S_3 hollow micro-spheres by HRTEM and GPA, confirming the existence of strain system and change of PL data. First principle calculation

uncovers that the lattice distortion causes the variation of S-3p and G-4p states and changes the band structure, further modifying the optoelectronic properties. All the results suggest that this novel strategy may be an attractive approach for tuning optoelectronic properties of sulfide semiconductors.

Acknowledgements

This work was supported by the Ministry of Science and Technology of China (973 Project No. 2013CB932901), and the National Natural Foundation of China (Nos. 11274066, 51172047, 51102050, U1330118). This project was sponsored by Shanghai Pujiang Program and “Shu Guang” project of Shanghai Municipal Education Commission and Shanghai Education Development Foundation (09SG01).

Notes and references

1. D. R. Cooper, N. M. Dimitrijevic and J. L. Nadeau, *Nanoscale*, 2010, **2**, 114-121.
2. J. Tian, Q. Zhang, L. Zhang, R. Gao, L. Shen, S. Zhang, X. Qu and G. Cao, *Nanoscale*, 2013, **5**, 936-943.
3. G. Zhu, Z. Cheng, T. Lv, L. Pan, Q. Zhao and Z. Sun, *Nanoscale*, 2010, **2**, 1229-1232.
4. S. Shen and Q. Wang, *Chemistry of Materials*, 2012, **25**, 1166-1178.
5. T. Wu, X. Zhou, H. Zhang and X. Zhong, *Nano Research*, 2010, **3**, 379-386.
6. C. Kumpf, R. Neder, F. Niederdraenk, P. Luczak, A. Stahl, M. Scheuermann, S. Joshi, S. Kulkarni, C. Barglik-Chory and C. Heske, *The Journal of chemical physics*, 2005, **123**, 224707.
7. Y. Yan, B. Xia, X. Qi, H. Wang, R. Xu, J.-Y. Wang, H. Zhang and X. Wang, *Chemical Communications*, 2013, **49**, 4884-4886.
8. X. Meng, J. A. Libera, T. T. Fister, H. Zhou, J. K. Hedlund, P. Fenter and J. W. Elam, *Chemistry of Materials*, 2014, **26**, 1029-1039.
9. R. Che, N. Bai and L.-M. Peng, *Applied physics letters*, 2003, **83**, 3561-3563.
10. H. Zhang, J. Huang, X. Zhou and X. Zhong, *Inorganic chemistry*, 2011, **50**, 7729-7734.
11. G. Shen, D. Chen, P.-C. Chen and C. Zhou, *ACS nano*, 2009, **3**, 1115-1120.
12. H. Liu, K. A. Antwi, N. Yakovlev, H. R. Tan, L. Ong, S. Chua and D. Chi, *ACS applied materials & interfaces*, 2014, **6**, 3501-3507.
13. P. Xu, L. Kang, N. H. Mack, K. S. Schanze, X. Han and H.-L. Wang, *Scientific reports*, 2013, **3**.
14. Y. Wu, C. Wadia, W. Ma, B. Sadtler and A. P. Alivisatos, *Nano letters*, 2008, **8**, 2551-2555.
15. K. Zhang and L. Guo, *Catalysis Science & Technology*, 2013, **3**, 1672-1690.
16. J.-S. Lee, Y.-H. Won, H.-N. Kim, C.-D. Kim and W.-T. Kim, *Solid state communications*, 1996, **97**, 1101-1104.
17. C.-H. Ho and H.-H. Chen, *Scientific reports*, 2014, **4**.
18. B. Liu and H. C. Zeng, *Small*, 2005, **1**, 566-571.
19. M. J. Hÿtch, J.-L. Putaux and J.-M. Pénisson, *Nature*, 2003, **423**, 270-273.
20. M. Hÿtch, F. Houdellier, F. Hÿe and E. Snoeck, *Nature*, 2008, **453**, 1086-1089.
21. H. Tian, J. Verbeeck, S. Brÿck, M. Paul, D. Kufer, M. Sing, R. Claessen and G. V. Tendeloo, *Advanced Materials*, 2014, **26**, 461-465.
22. Z. A. Alahmed, *Solid State Sciences*, 2013, **21**, 11-18.
23. B. Amin, T. Kaloni and U. Schwingenschlÿgl, *RSC Advances*, 2014, **4**, 34561-34565.